Research Article Vol. 32, No. 5 / 26 Feb 2024 / Optics Express 7030
Optics EXPRESS

Three-photon and four-photon absorption in lithium niobate measured by the Z-scan technique

IMENE BENABDELGHANI,[1,2] GYÖRGY TÓTH,[1,2] GERGŐ KRIZSÁN,[1,2,3] GÁBOR BAZSÓ,[4] ZSUZSANNA SZALLER,[4] NELSON MBITHI,[5] PÉTER RÁCZ,[4] PÉTER DOMBI,[4] GYULA POLÓNYI,[1,3] AND JÁNOS HEBLING[1,2,*]

[1]*Szentágothai Research Centre, Ifjúság street 20, 7624, Pécs, Hungary*
[2]*University of Pécs, Ifjúság Street 6, 7624, Pécs, Hungary*
[3]*HUN-REN – PTE High Intensity Terahertz Research Group, Ifjúság Street 6, 7624, Pécs, Hungary*
[4]*Wigner Research Center for Physics, Institute for Solid State Physics and Optics, H-1121 Budapest, Hungary*
[5]*Garissa University, Garissa, Kenya*
[*]*hebling@fizika.ttk.pte.hu*

Abstract: Open-aperture Z-scan measurements have been carried out to investigate the three-photon (3 PA) and four-photon absorption (4 PA) coefficients at 800 nm and 1030 nm wavelengths, respectively in congruent and stoichiometric lithium niobate (cLN, sLN) with different concentrations of Mg doping. The laser pulse duration at the two wavelengths were 40 and 190 fs. The peak intensity inside the crystals varied between approximately 110 and 550 GW/cm^2. The 3 PA and 4 PA coefficients were evaluated using a theoretical model and the results suggest that their minima are at or around the Mg doping level corresponding to the threshold for suppressing photo-refraction for both cLN and sLN. This result can be attributed to the contribution of crystal defects to the 3 PA and 4 PA processes. Furthermore, the 4 PA at 1030 nm exhibited greater nonlinear absorption than the 3 PA at 800 nm under the same intensity level. Possible reasons for this unexpected behavior are discussed. Overall, comparing the 3 PA and 4 PA values of these crystals will enable for selection of the optimum composition of LN crystal for efficient THz generation and for other nonlinear optical processes requiring high pump intensities.

1. Introduction

The terahertz range (~0.1–10 THz) of the electromagnetic spectrum has drawn significant attention due to its potential for fundamental physics and a wide variety of applications [1]. Over the past two decades, optical rectification (OR) of femtosecond near-infrared laser pulses in lithium niobate ($LiNbO_3$, LN) has become the most widely used effective method for generating both high-energy broadband terahertz (THz) pulses [2–4] and narrowband radiation [5–7] in the 0.1–2 THz frequency range. Due to the more than two-fold difference between the indices of refraction for near-infrared (used for pumping) and the THz waves, high pump-to-THz conversion efficiency was achieved through quasi-phase matching by periodically poling [8], and velocity matching by tilted-pulse-front pumping [9], for narrowband and broadband pulse generation, respectively. Recently, the nonlinear absorption phenomenon, observed in a variety of materials [10], especially multi-photon absorption (MPA) [11,12], and free-carrier absorption (FCA)) [12,13] has received considerable interest due to its potential strong negative effect on the efficiency of frequency conversion processes, peculiarly OR. Lithium niobate crystal was first fabricated in Bell Laboratories in the mid-'60s. It is insoluble in water and transparent in a wavelength range of approximately 350 and 5200 nm. Possessing a trigonal crystal structure

#505995 https://doi.org/10.1364/OE.505995
Journal © 2024 Received 14 Sep 2023; revised 14 Dec 2023; accepted 15 Dec 2023; published 13 Feb 2024

Optics EXPRESS

[14] and a large bandgap of around 3.8 eV [15,16]. This material exhibits outstanding properties for nonlinear optical applications. It demonstrates a high damage threshold of 204 GW/cm^2 for 1 ps-long pulses with a repetition rate of 10 kHz and 2.4 TW/cm^2 threshold intensity at 1030 nm, 330 fs, and 20 kHz repetition rate [17], and a high nonlinear optical coefficient of approximately 30 pm/V for frequency conversion processes on the near-infrared range [14], and has a fascinating value of 160 pm/V for the OR process [18]. LN is grown from its melt of Li_2O and Nb_2O_5. Since Nb ions tend to substitute for Li ions, maintaining a homogeneous crystal with constant composition requires the use of a so-called congruent melt, containing 48.45 mol% Li_2O and 51.55 mol% Nb_2O_5 [19]. Over the last two decades, stoichiometric LN (sLN) with excellent homogeneity has also become available. Both congruent LN (cLN) and sLN exhibit photorefractive properties, which are disadvantageous for frequency conversion applications. These can be suppressed by e.i. Mg doping. The threshold Mg doping for suppressing photorefraction is over 5 mol% for cLN, and about 0.6 mol% for sLN. At the intensity level of 100 GW/cm^2 for the pump laser beam used in nonlinear optical frequency conversion applications, such as OR, both MPA and nonlinear refraction (NLR) can be significant. A straightforward technique for investigating the MPA and NLR properties of materials is the z-scan technique, introduced by Sheik-Bahae et al. [20]. A simple transmission measurement was used to determine the 2 PA [21], while the z-scan technique has been applied to evaluate the 3 PA [22] in lithium niobate, as well as 2 PA in lithium tantalate crystal [23]. To the best of our knowledge the 4 PA of LN has not been measured yet using the z-scan technique. An early estimated value of the 4 PA coefficient of LN was deduced from the saturation of the THz pulse generation efficiency with increasing pump intensity [24]. Recently, a simple transmission measurement was used to determine the 4 PA coefficient of sLN [25].

The aim of the research reported in this paper was to determine the 3 PA, and 4 PA coefficients at 800 and 1030 nm laser wavelengths in both cLN and sLN by open aperture z-scan measurement. The dependence of the MPA on the Mg doping concentration was also investigated for both ordinary and extraordinary polarized light. The 3 PA and 4 PA coefficients of these crystals were numerically determined from the measured z-scan curves. Knowledge of these MPA coefficients are crucial for the accurate design and optimization of frequency conversion, electro-optical, and other photonic devices working in both the infrared and THz ranges.

2. Experimental details

For measuring the MPA coefficients of LN, the standard open aperture z-scan setup has been carried out. As it is illustrated in Fig. 1 the experimental setup consisted of a Ti: sapphire laser (Newport-Spectra Physics) producing 40 fs long pulses at 800 nm, or an Yb laser (Pharos, Light Conversion) producing 190 fs long pulses at 1030 nm at 1 kHz repetitions rate, a combination of a halfwave plate and a thin film polarizer for fine adjustment of the power of the laser beam at the sample, and a lens with an 500 mm or 400 mm focal length for focusing. The investigated LN crystal was mounted on a motorized linear stage to move it along the beam propagation direction (z-axis) around the focal plane. A lens with 150 mm focal length was used after the focal plane to eliminate the divergence of the laser beam. A large-area (Ø 9.5 mm) Si optical power sensor (Thorlabs S120C/PM100) and a Si photodetector (Thorlabs DET100A2, 75 mm^2) were used for measuring the energy of the transmitted laser beams through the LN sample, respectively.

The $w(z)$ 1/e^2 radius of the focused laser beam has been carefully measured both in the horizontal and vertical direction by the knife-edge technique at many positions along the propagation direction of the laser beam (z-axis). The sizes determined in this way are plotted in Fig. 2(a) and (b). Both for horizontal and vertical sizes, the measurement results were fitted

Optics EXPRESS

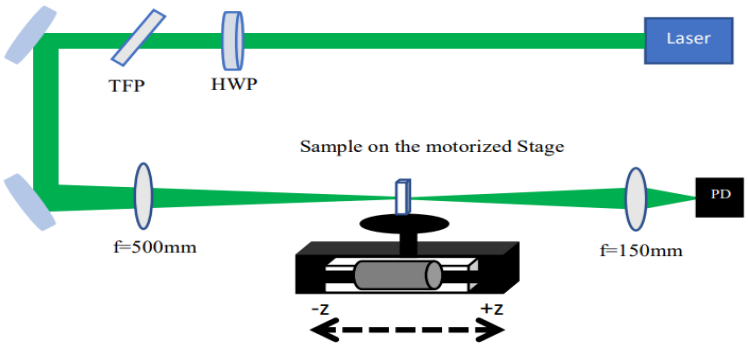

Fig. 1. Schematic of the z-scan experimental setup. HWP: half-wave plate, TFP: thin film polarizer, PD: photodiode, +z shows the positive direction toward the detector, -z shows the negative direction toward the focusing lens.

according to Eq. (1).

$$w(z) = w_0\sqrt{1 + \left(\frac{M^2\lambda}{\pi w_0^2}\right)^2 (z - z_0)^2} \tag{1}$$

The fitting parameters were the w_0 spot sizes, the M^2 parameters, and the z_o positions of the focus. The $z_R = \pi w_0^2/M^2\lambda$ Rayleigh ranges were also obtained for both the horizontal (H) and vertical (V) directions. From the Rayleigh ranges belonging to the horizontal and vertical directions a single z_R was associated to the laser beam according to $z_R = \sqrt{z_{RH} \cdot z_{RV}}$. The beam parameters determined by this way are indicated in Table 1 and Table 2 for the 800 nm and 1030 nm wavelengths, respectively. It can be seen, that for the 800 nm beam, the horizontal and vertical sizes are close (within 10%) to each other, and the M^2 value is rather close to 1.0. For the 1030 nm beam, the deviations are about a factor of two larger.

Table 1. Beam parameters of the 0.8 µm beam determined by the knife-edge method.

		spot size w_0 (um)	M^2 parameter	Rayleigh range (mm)
Broad range	Horizontal	36	1.48	3.61
	Vertical	30	1.23	2.96
Narrow range	Horizontal	32	1.36	3.03
	Vertical	28	1.16	2.68

Table 2. Beam parameters of the 1.03 µm beam determined by the knife-edge method.

		spot size w_0 (um)	M^2 parameter	Rayleigh range (mm)
Broad range	Horizontal	69	1.69	8.65
	Vertical	57	1.18	8.64
Narrow range	Horizontal	69	1.60	8.66
	Vertical	56	1.16	8.60

Since a detailed investigation indicated a slight dependence of the obtained fitting parameters on the z range of the fittings, the fittings were repeated for a narrower z range corresponding to about $\pm 3z_R$, where the value of the z-scan curves differs noticeably from 1 (see Fig. 5 and Fig. 7). These parameters, indicated in Table 1 and Table 2 were used in the simulation of the z-scan curves. In Fig. 2(b) a small difference in the position of the focal plane can be seen for

Optics EXPRESS

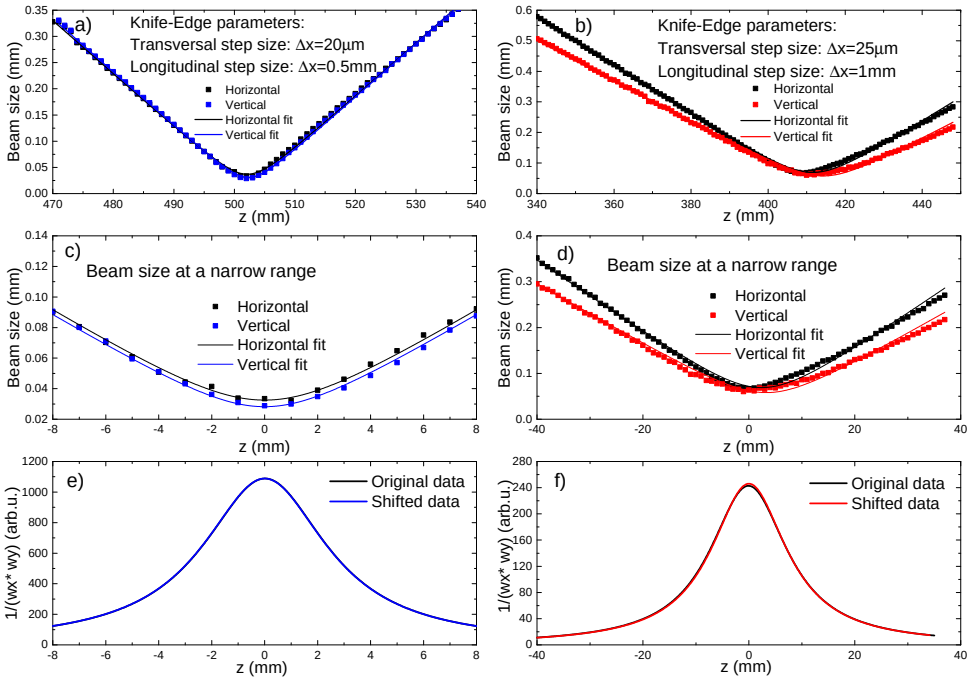

Fig. 2. The measured horizontal and vertical spot sizes versus the propagation coordinate for 0.8 μm (a) and 1.03 μm (b) beams. The same indicated for an about $\pm 3z/z_R$ range (c,d). Relative intensity curves calculated with the original and the shifted data (e,f).

the horizontal and vertical scans. Figure 2(a) shows a similar but smaller effect. For both cases we applied an appropriate (0.5 mm for 0.8 μm beam and 1 mm for 1.03 μm beam) relative shift of the "horizontal" and "vertical" curves in order to achieve exactly the same position of the beam-waists. The curves obtained in this way are indicated in Fig. 2(c) and (d). We estimated the effect of neglecting the slightly different positions of the horizontal and vertical beam-waist as follow: $1/(w_H(z) \times w_V(z))$ was calculated with the original fitting curves and with the modified ones. The results are shown in Fig. 2(e) and (f). In Fig. 2(e) the two curves are indistinguishable, in Fig. 2(f) the difference between the maxima of the two curves is less than 1%. So we can neglect the effect of the shift of the curves on the beam intensity function.

The samples used in the experiment are listed in Table 3**.** Both cLN and sLN crystals having different Mg doping concentrations were selected. The measurements have been performed at 110, 255, 290, and 555 GW/cm^2 pump intensity (inside the sample) for the 0.8 μm beam, and 180 GW/cm^2 pump intensity for the 1.03 μm beam. The samples were scanned in the vicinity of the lens focus ($z = 0$) starting from a position ahead of the focus (negative z) and moving toward a position behind the focus (positive z). For the determination of the MPA coefficients, the application of the open aperture Z-scan measurement was intended. However, the measured z-scan curves show slight asymmetry (see Fig. 3(a)), an effect attributed temporarily to self-focusing caused by nonlinear refraction, or photo-refraction, indicating that the detector was not large enough. Because of this we separated the effect of MPA and self-focusing by applying the subtraction method described in Ref. [26]. In this way we obtained symmetric curves as it is indicated in Fig. 3(b). The minima of these modified z-scan curves have been fitted by varying the 3 PA (for the 0.8 μm beam) or 4 PA (for the 1.03 μm beam) coefficients in our nonlinear pulse propagation model. (Since LN has a band-gap of about 3.8 eV, the maximum wavelength where

Optics EXPRESS

3 PA is possible is about $\lambda_{3PA} = \frac{3hc}{E_g} = 980\ nm$). In each case, five measured data points with the lowest transmission values were considered for fitting by the least-square method, and the MPA coefficient was the only fitting parameter.

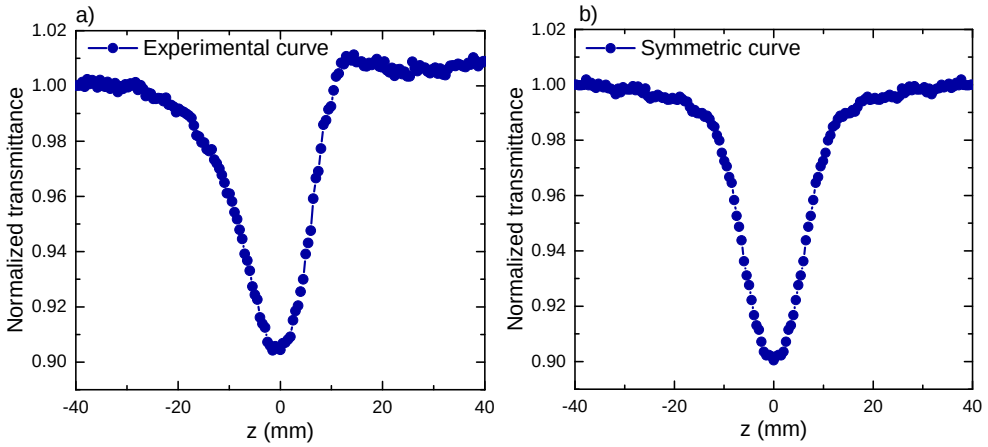

Fig. 3. As an example, the directly measured z-scan curve (a), measured with 1.03 µm beam and the symmetrized curve (b) is shown in the case of sLN:1.50% Mg crystal for ordinary polarization.

Table 3. Parameters of the studied samples

Crystal	Notation of sample	Mg doping level (mol%)	Size (x,z) (mm)	Thickness (mm)
$LiNbO_3$	sLN:4.18% Mg	4.18	7×8	0.610
	sLN:1.50% Mg	1.50	3×6	0.600
	sLN:0.67% Mg	0.67	4.15×5	0.605
	cLN	0.0	5×10	0.600
	cLN:1.0% Mg	1.0	5×6	0.601
	cLN:6.0% Mg	6.0	12×6	0.600

Figure 4 presents the measured absorption of all the investigated samples with different Mg-doping concentrations around the UV absorption edge both for the ordinary (left column) and extraordinary (right column) polarization. (The detector saturated at an absorbance value larger than 3, corresponding to about 120 cm^{-1} absorption coefficient.) We indicated the wavelengths three-times smaller than 800 nm (green dashed line to the left) and 1030 nm (green dashed line to the right). According to this, at the 800 nm case, the three-photon energy is in the saturated region, thus it is sufficient to excite the valence electrons to the conduction band, which is not the case for 1030 nm. As a result, we can state with certainty that the dominant effect at 800 nm is the 3 PA, and at 1030 nm is the 4 PA.

Optics EXPRESS

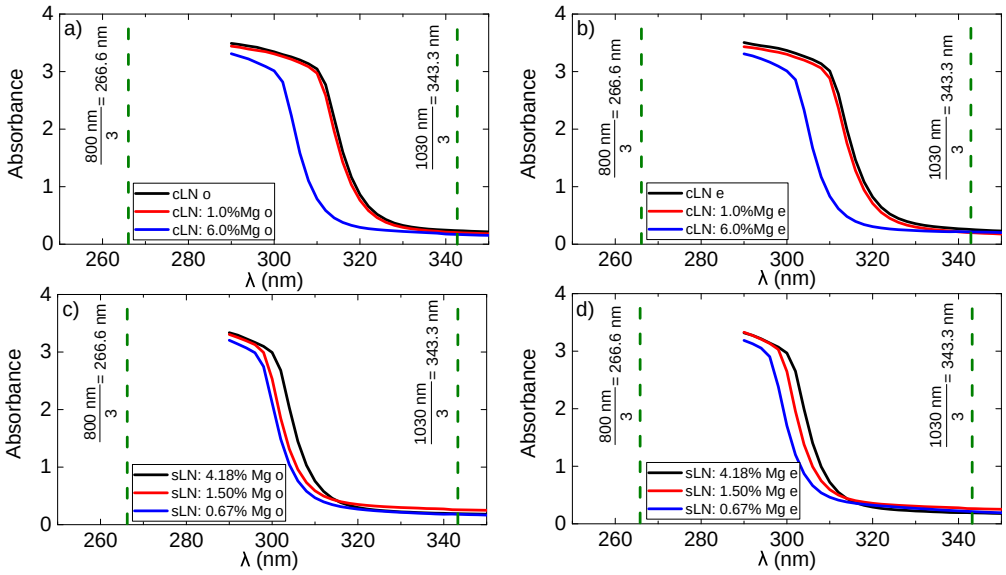

Fig. 4. UV absorption spectra for all the investigated crystals for both ordinary and extraordinary polarized light.

3. Numerical model

In order to determine the β_n n$^{\text{th}}$-order MPA coefficient a pulse propagation model, similar to Ref. [27] was used. For every z_c position of the LN crystal, at the inner side of the entrance surface of the crystal the following intensity distribution of the laser pulse was assumed:

$$I(z=0,x,y,t;z_c) = \frac{4n_0}{(n_0+1)^2} I_0 \frac{w_{0H}}{w_{0H}(z_c)} \frac{w_{0V}}{w_{0V}(z_c)} \exp\left(-\frac{2x^2}{w_{0H}^2(z_c)}\right) \exp\left(-\frac{2y^2}{w_{0V}^2(z_c)}\right) \exp\left(-\frac{4\ln(2)t^2}{\tau^2}\right), \tag{2}$$

where $w_{0H,0V}(z_c) = w_{0H,0V}\sqrt{1+\frac{z^2}{z^2_{RH,RV}}}$,$\tau$ is the FWHM duration of the laser pulse, and n_0 is the phase refractive index. The I_0 peak intensity of the laser beam at the beam-waist was calculated according to Eq. (3)

$$I_0 = \frac{4E_l\sqrt{\ln(2)}}{\pi^{3/2}\tau w_{0H} w_{0V}}, \tag{3}$$

where E_l is the energy of the laser pulse before entering the crystal.

The first term on the right side of Eq. (2) takes into account the reflection loss at the entrance surface.

The complex electric field envelope was determined inside the crystal at the beginning position as the following:

$$A(z=0,x,y,t;z_c) = \sqrt{\frac{2I(z,x,y,t)}{\varepsilon_0 c n_0}}, \tag{4}$$

Optics EXPRESS

where ε_0 is the vacuum permittivity and c is the speed of the light in vacuum. For description of the pulse propagation inside the crystal,

$$\frac{dA(z,x,y,t;z_c)}{dz} = -\frac{\beta_n}{2^n}(\varepsilon_0 c n_0)^{n-1}A^{2n-1}(z,x,y,t;z_c) + \; F^{-1}\left\{F\left\{i\frac{n(\omega)\omega}{c}A(z,x,y,\omega;z_c)\right\}\right\}, \quad (5)$$

The differential equation was solved. Here F and F^{-1} are the Fourier- and the inverse-Fourier-transformation, respectively. The first term of the differential equation describes the nth-order nonlinear absorption and the second term describes the dispersion of the crystal.

The z-scan transmission curve can be determined according to

$$T(z_c) = \frac{\int_{-\infty}^{\infty}\int_{-\infty}^{\infty}\int_{-\infty}^{\infty}|A(z=L,x,y,t;z_c)|^2 \mathrm{d}x\mathrm{d}y\mathrm{d}t}{\int_{-\infty}^{\infty}\int_{-\infty}^{\infty}\int_{-\infty}^{\infty}|A(z=0,x,y,t;z_c)|^2 \mathrm{d}x\mathrm{d}y\mathrm{d}t} \quad (6)$$

where L is the thickness of the crystal.

4. Results

4.1. Z-scan curves obtained for 800 nm laser

With 800 nm laser measurement only at extraordinary polarization was performed. The measured results after symmetrization and normalization, together with the fitting curves are plotted in Fig. 5 both for the cLN (left column) and sLN (right column) samples with different Mg-doping concentration. The graphs are ordered in both columns according to the crystal defect concentration: the graphs belonging to the highest defect concentrations are on the first raw, and the graphs belonging to the lowest defect concentrations are on the last raw. The indicated intensity values for the different curves mean the peak intensity at the beam center inside the samples**.** It can be seen that, – with the exception of the smallest intensity for the sLN:4.18% Mg and cLN:1.0% Mg samples, – a good quality fitting of the experimental values (dots) are possible for all cases. According to the indicated 3 PA coefficients resulting the best fit, the 3 PA coefficients have a maximum at about 290 GW/cm^2 for all the investigated crystal compositions.

Figure 6(a) and (b) show the measurement and fitting results at 290 GW/cm^2 intensity for sLN and cLN crystals, respectively. The results indicate relatively small composition dependence, but for both sLN and cLN the 3 PA coefficient is smallest for the compositions (sLN:0.67% Mg and cLN:6.0% Mg) having a Mg doping concentration closest to the photorefraction suppression threshold [16,28].

In Fig. 6(a), a 0.5% increase in the measured transmission can be observed, followed by the valley corresponding to 3 PA. The possible reason for this increment could be due to the linear absorption of some contamination on the sample during the growth, or it could be related to the saturation of a transition state caused by pumping, or even more complex processes could be behind it. In the case of the z-scan measurement of malachite crystal, various nonlinear mechanisms was necessary to be considered into the fitting model for this reason [29].

4.2. Z-scan curves obtained for 1030 nm laser

With 1030 nm laser measurement only at one intensity (180 GW/cm^2), but for both ordinary and extraordinary polarizations was performed. The measured results after symmetrization and normalization, together with the fitting curves are plotted in Fig. 7 both for the cLN (left column) and sLN (right column) samples with different Mg-doping concentration. The results for the extraordinary polarization are indicated in the first raw, and for the ordinary one in the second raw, respectively.

At first glance, it seems obvious that the measured Z-scan curve does not match very well with the fitting curve assuming 4 PA, contrary to the case of 0.8 μm wavelength. In most cases, the

Optics EXPRESS

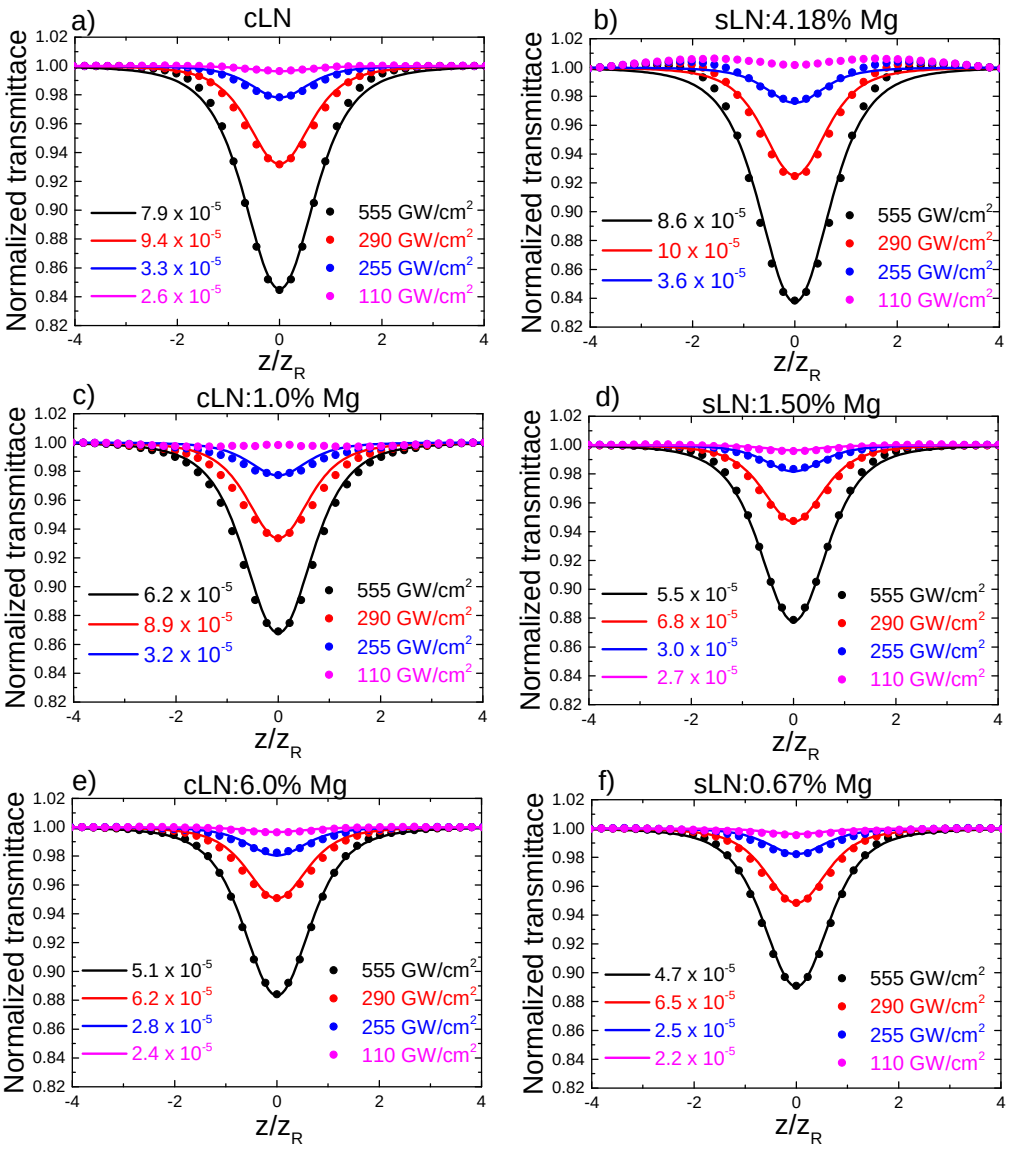

Fig. 5. Result of z-scan measurements (dots) together with fitting curves for different crystals and laser intensities. The 3 PA coefficients resulting the best fitting are indicated. β_3 is measured in $\mathrm{cm}^3/\mathrm{GW}^2$.

width of the measured curves is significantly larger than that of the theoretical fitting curves. Furthermore, inspecting the z-scan curves measured at extraordinary polarization, it is very surprising that, contrary to the fact that at 1.03 µm only 4 PA is possible, while at 0.8 µm the usually stronger 3 PA is the lowest order MPA, the absorption for 1.03 µm at 180 GW/cm^2 is between the absorptions obtained for 0.8 µm at 110 and 255 GW/cm^2, respectively (see Fig. 5). For the sLN:4.18% Mg crystal the absorption is even significantly larger at 1.03 µm than at 0.8 µm. In case where the defect concentration is the highest: sLN:4.18% Mg, and cLN (ordinary pol.) the measured transmission valleys are wider than the fitting window causing mediocre fittings. As they do not possess practical value as their THz absorption (sLN:4.18% Mg), or

Optics EXPRESS

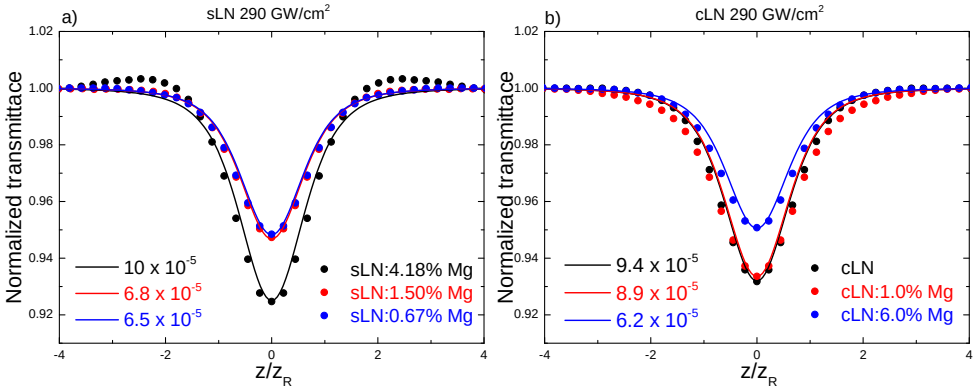

Fig. 6. Result of the z-scan measurements (dots) together with fitting curves for sLN (a) and cLN (b) at 290 GW/cm^2 for different crystal compositions. β_3 is measured in units of cm^3/GW^2.

their photorefraction (cLN without doping) is unusably high [30], they have been left out from evaluation.

Similar to the 0.8 µm case, for 1.03 µm the absorption also has minimum at a magnesium doping concentration corresponding to the photorefaction suppression threshold. However, for 1.03 µm the magnesium doping dependence is much stronger than for 0.8 µm. The z-scan curves measured at ordinary polarization indicate significantly larger absorption than the ones measured for extraordinary polarization. This is especially true for the crystals (cLN and sLN:4.18% Mg) having magnesium doping concentration farthest from the photorefraction suppression threshold.

These observations indicate that for 1.03 µm, nonlinear absorption is primarily not caused by genuine 4 PA. Nevertheless, we determined 'effective' 4 PA values through fitting, which can be used for designing nonlinear optical applications at the intensities used during measurement.

All the determined 3 PA and "effective" 4 PA coefficients are collected into Table 4. One clear observation having practical importance is that for 0.8 µm and less than 300 GW/cm^2 intensity (the range what is usually applied for pumping LN THz sources) there is almost no intensity dependence.

Table 4. Three-photon absorption coefficients and four-photon effective absorption coefficients of all samples for ordinary and extraordinary polarization

	β_3 ($\times 10^{-5}$ cm^3/GW^2) 800 nm				β_4 ($\times 10^{-7}$ cm^5/GW^3) 1030 nm	
	Extraordinary				Ordinary	Extraordinary
	110 GW/cm^2	255 GW/cm^2	290 GW/cm^2	555 GW/cm^2	180 GW/cm^2	
sLN: 4.18% Mg	-	3.6	10	8.6	-	-
sLN: 1.50% Mg	2.7	3.0	6.8	5.5	44	4.0
sLN: 0.67% Mg	2.2	2.5	6.5	4.7	33	2.9
cLN	2.6	3.3	9.4	7.9	-	5.7
cLN: 1.0% Mg	-	3.2	8.9	6.2	14	4.8
cLN: 6.0% Mg	2.4	2.8	6.2	5.1	12	3.6

Optics EXPRESS

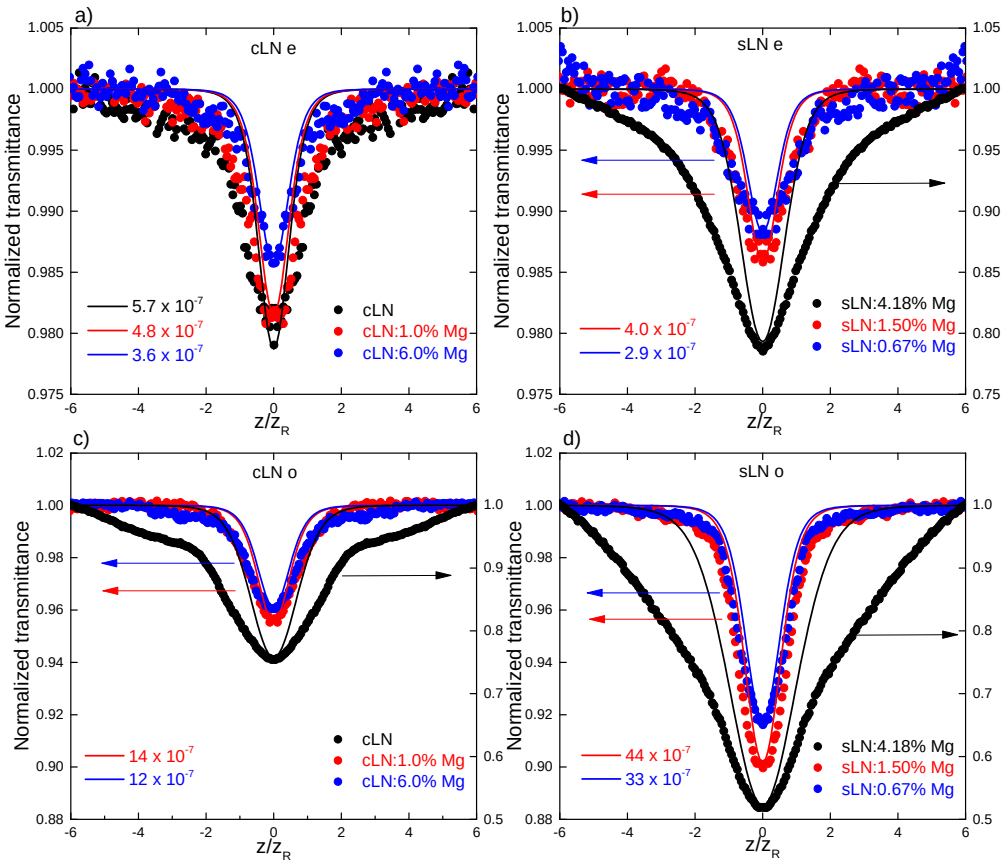

Fig. 7. Result of the z-scan measurements (dots) together with fitting curves for cLN (a, c) and sLN (b, d) crystals with different Mg doping levels at 180 GW/cm^2 laser intensity for extraordinary (a,b) and ordinary (c,d) polarization. β_4 is measured in cm^5/GW^3. It can be realized that the fit is poor and not able to determine the 4 PA in case of sLN:4.18% Mg and cLN, but since the doping level is not practical for the applications due to the corresponding high THz absorption or high photorefraction (sLN:4.18%Mg and cLN, respectively) [30], we leave it out from the evaluation.

5. Discussion

Firstly, we have to notice a few facts on the accuracy of the measurements of the MPA coefficients. The determination of the MPA coefficient is based on the measurement of the relative change of the transmission. As it is demonstrated by i.e. Fig. 5, using lock-in, or other averaging technique, this can be measured with better than 1% accuracy. However, the calculated MPA coefficient depends on the absolute value of the intensity, too, and the determination of the intensity is possible only with much less accuracy. The reason is that the determination of the intensity is usually based on Eq. (3), which is exact only for beams with perfectly Gaussian temporal and spatial distribution. Furthermore, it is difficult to measure the pulse duration and the beam-waists with better than 5% accuracy. Taking into account this and the feature of the error propagation, the typical accuracy of the intensity is $\pm 20 \div \pm 50\%$. This results in about n-1 times larger uncertainty in the determination of the nth-order MPA coefficient.

We start the comparison of our results with previous findings by discussing the 4 PA coefficient, since previous measurements of the 4 PA coefficient for LN, having a composition essentially

Optics EXPRESS

identical to our sample and the same laser polarization, are available. Reference [25] reports a β_4 value of 3.0×10^{-6} cm^5/GW^3 4 PA coefficient for Mg-doped sLN measured using an 1050 nm laser with an intensity of 200 GW/cm^2 and extraordinary polarization. Although the doping concentration is not mentioned, it is likely to have been around 1%, as such crystals typically supplied. This reported 4 PA coefficient value is approximately one order of magnitude higher than our measured values for 0.7% Mg doped sLN ($\beta_4 = 2.9 \times 10^{-7}$ cm^5/GW^3) and 1.5% Mg doped sLN ($\beta_4 = 4.0 \times 10^{-7}$ cm^5/GW^3) crystals (see Table 4). We believe that this discrepancy cannot be solely attributed to the accuracy of laser intensity measurements in the two cases. Rather, the use of a laser with five times longer laser pulse duration (1 ps) and a 50 times larger repetition rate (50 kHz) used in the measurement reported in Ref. 25 could lead to an apparently larger 4 PA coefficient. Nearly three decades ago, Hinari et al. observed nonlinear absorption in cLN using a cw Ar-ion laser at 514 nm [31]. Using Z-scan method they measured a substantial nonlinear absorption coefficient value of, $\beta = 5 \times 10^6$ cm/GW^2. Subsequent measurements by Pálfalvi et al., using similar techniques but with photorefraction suppressed LN crystals, yielded coefficients that were three orders of magnitude smaller but still significantly large. For example, in 0.7% Mg-doped sLN, they found β values of 1.7×10^3 cm/GW^2 and 0.55×10^3 cm/GW^2 for extraordinary and ordinary polarization, respectively. In these cases, due to the relatively low (cw) laser intensities used, direct two-photon absorption is unlikely to be the real cause of the observed nonlinear absorption. Instead, two-step processes involving crystal defects are likely responsible. In Ref. [31] Nb^{4+} and O^- intrinsic defects was named as possible intermediate levels involved in this two-step process.

In both our experiments and those of Ref. [25], a Yb-laser with a wavelength of 1.03 μm was utilized, and so, because of the small photon energy, neither real two-photon absorption, neither two-step, intermediate level mediated two-photon absorption are possible. However, it's worth noting that (non-phase matched) second-harmonic generation (SHG) could lead to the generation of intense pulses inside the examined LN crystals at 515 nm. This is because, for ordinary input polarization, the l_c SHG coherence length of the ooe (ordinary + ordinary → extraordinary) SHG process is longer than 100 μm for a few investigated crystal compositions (see Table 5). We have checked the importance of the 515 nm light generated in this way by employing our Z-scan setup and positioning the sLN:4.18% Mg crystal in the focal spot of the Yb-laser pulses with an intensity of 180 GW/cm^2. We observed SHG with an external efficiency of 6–8%. Although, the coherence length for the eee process is significantly shorter, and the observed SHG efficiency for extraordinary-polarized 1.03 μm wavelength was approximately 100 times smaller, a 100-200 MW/cm^2 intensity of the generated 515 nm radiation can be enough for non-negligible two-photon absorption. Given that the nonlinear absorption observed in Ref. [28] and [31] is attributed to a two-step process involving crystal defects, it is likely that the absorption depends not only on light intensity but also on light fluence. Therefore, longer pulse durations and higher repetition rates can lead to increased additional absorption through the two-step process involving crystal defects. This could explain the observed one-order-larger 4 PA coefficient in Ref. [25] compared to our observations. The additional absorption due to this extra mechanism could provide an explanation for the significantly larger measured 4 PA coefficient observed for ordinary polarization (with stronger SHG) compared to the case of extraordinary polarization (see Table 4). It also clarifies why the 4 PA coefficient is at its largest (see Table 4) for crystal compositions (cLN and sLN:4.18% Mg) that exhibit the highest defect concentration, representing an intermediate state of the two-step absorption process. In cLN crystals, beside the ≈1 mol% antisite Nb ions (Nb_{Li}, Nb on Li site), about 4 mol% charge compensating Li vacany is present, while in sLN:4.18% Mg a variety of extrinsic and intrinsic defects may occur on the percentage scale, such as Mg either on Li or Nb site and Li vacancy.

It is important to notice, that valence – conduction band transition induced by 4 PA of 1030 nm, and 2 PA of 515 nm laser and SHG pulse, in the present of the mentioned crystal defects can

Optics EXPRESS

Table 5. Calculated coherence length (l_c) for second harmonic generation (SHG) in both oo-e and ee-e SHG processes in a few crystal compositions. n_o and n_e are the refractive indices for ordinary and extraordinary polarizations, respectively.

Crystal	Wavelength (μm)	n_o	n_e	Ref	Process	l_c (μm)
cLN	1.03	2.2351	2.1584	[34]	oo-e	26.54
	0.515	2.3356	2.2448		ee-e	2.98
	0.8	2.2541	2.1749		oo-e	2.78
	0.4	2.4317	2.3260		ee-e	1.32
cLN:5.0% Mg	1.03	2.2319	2.1506	[35]	oo-e	533
	0.515	2.3283	2.2324		ee-e	3.14
	0.8	2.2527	2.1683		oo-e	3.06
	0.4	2.4307	2.3180		ee-e	1.33
sLN	1.03	2.2370	2.1567	[36]	oo-e	29.59
	0.515	2.3410	2.2457		ee-e	2.89
	0.8	2.2571	2.1745		oo-e	4.40
	0.4	2.4089	2.3025		ee-e	1.56
sLN:4.5% Mg	1.03	2.2257	2.1453	[37]	oo-e	157.01
	0.515	2.3220	2.2274		ee-e	3.13
	0.8	2.2465	2.1634		oo-e	2.92
	0.4	2.4249	2.3150		ee-e	1.31
sLN:3.3% Mg	1.03	2.2292	2.1454	[37]	oo-e	136.96
	0.515	2.3260	2.2274		ee-e	3.14
	0.8	2.2509	2.1639		oo-e	3.17
	0.4	2.4330	2.3139		ee-e	1.33
sLN:2.0% Mg	1.03	2.2326	2.1451	[37]	oo-e	43.71
	0.515	2.3294	2.2267		ee-e	3.15
	0.8	2.2538	2.1636		oo-e	3.46
	0.4	2.4330	2.3116		ee-e	1.35
sLN:0.78% Mg	1.03	2.2342	2.1456	[37]	oo-e	36.16
	0.515	2.3306	2.2271		ee-e	3.15
	0.8	2.2555	2.1639		oo-e	3.36
	0.4	2.4389	2.3150		ee-e	1.32

effectively create different type of polarons [32]. These polarons has broad absorption bands in the visible, and made possible 2 PA of the 1030 nm laser pulse. The lifetime of the polarons makes possible their accumulation at 1 kHz repetition rate used in our experiments, and even more at the 50 kHz repetition rate used in Ref. 25.

At 0.8 μm wavelength, the SHG coherence length for extraordinary polarization is only 1.0 – 1.5 μm, resulting in negligible SHG. Consequently, the additional absorption through the two-step process is also negligible. This could be a contributing factor to the 3 PA at 0.8 μm not being stronger than the 4 PA at 1.03 μm wavelength. Additionally, it's worth noting that when investigating the intensity dependence of different-order multi-photon absorption (MPA) in a chalcogenide glass with a 2.5 eV bandgap energy, it was found to surpass the 4 PA of the 3 PA at intensities greater than 30 GW/cm^2 [33]. In light of these findings, it wouldn't be surprising if a similar trend occurs, as our results indicate, in the 100–200 GW/cm^2 range for LN with a 3.8 eV bandgap energy.

Optics EXPRESS

6. Conclusion

In conclusion, our study employed open-aperture Z-scan measurements to explore the determination of three-photon (3 PA) and four-photon absorption (4 PA) coefficients in congruent and stoichiometric lithium niobate (cLN, sLN) with varying concentrations of Mg doping, utilizing laser pulses at 800 nm and 1030 nm wavelengths. Remarkably, we observed that the 3 PA and 4 PA coefficients exhibited distinctive variations at different Mg doping concentration with different intensities. Both cLN and sLN displayed minima in their absorption coefficients at a specific Mg doping concentration, corresponding to the point at which photo-refraction was effectively suppressed. This finding indicating the role of the interplay of second harmonic and the defect center related polarons, shedding light on the underlying mechanisms governing these nonlinear optical phenomena. Furthermore, our investigation revealed a difference in the nonlinear absorption behavior between 3 PA at 800 nm and 4 PA at 1030 nm, with the latter exhibiting greater absorption under similar intensity levels, the analysis of 3 PA and 4 PA coefficients in these lithium niobate crystals holds significant promise for selecting the most suitable crystal type for efficient terahertz (THz) generation and other nonlinear optical processes that demand high pump intensities.

Funding. National Research, Development and Innovation Office (2018-1.2.1-NKP-2018-00009, 2018-1.2.1-NKP-2018-00010).

Acknowledgments. The authors would like to express their gratitude to László Kovács for his contributions to this work. We acknowledge support from the National Research, Development and Innovation Office of Hungary (Projects 137373, TKP-2021-NVA-04).

Disclosures. The authors declare no conflicts of interest.

Data availability. Data underlying the results presented in this paper are not publicly available at this time but may be obtained from the authors upon reasonable request.

References

1. M. Tonouchi, "Cutting-edge terahertz technology," Nat. Photonics **1**(2), 97–105 (2007).
2. J. A. Fülöp, Z. Ollmann, C. Lombosi, *et al.*, "Efficient generation of THz pulses with 0.4 mJ energy," Opt. Express **22**(17), 20155–20163 (2014).
3. M. Nagai, M. Jewariya, Y. Ichikawa, *et al.*, "Broadband and high power terahertz pulse generation beyond excitation bandwidth limitation via χ(2) cascaded processes in LiNbO3," Opt. Express **17**(14), 11543–11549 (2009).
4. B. Zhang, Z. Ma, J.-L. Ma, *et al.*, "1.4 mJ high energy terahertz radiation from lithium niobates," Laser Photonics Rev. **15**(3), 1–11 (2021).
5. S. Carbajo, J. Schulte, X. Wu, *et al.*, "Efficient narrowband terahertz generation in cryogenically cooled periodically poled lithium niobate," Opt. Lett. **40**(24), 5762–5765 (2015).
6. F. Ahr, S. W. Jolly, N. H. Matlis, *et al.*, "Narrowband terahertz generation with chirped-and-delayed laser pulses in periodically poled lithium niobate," Opt. Lett. **42**(11), 2118–2121 (2017).
7. F. Lemery, T. Vinatier, F. Mayet, *et al.*, "Highly scalable multicycle terahertz production with a homemade periodically poled macrocrystal," Commun. Phys. **3**(1), 150 (2020).
8. Y.-S. Lee, T. Meade, V. Perlin, *et al.*, "Generation of narrow-band terahertz radiation via optical rectification of femtosecond pulses in periodically poled lithium niobate," Appl. Phys. Lett. **76**(18), 2505–2507 (2000).
9. J. Hebling, G. Almási, I. Z. Kozma, *et al.*, "Velocity matching by pulse front tilting for large area THz-pulse generation," Opt. Express **10**(21), 1161–1166 (2002).
10. E. W. Van Stryland, M. Sheik-Bahae, A. A. Said, *et al.*, "Characterization of nonlinear optical materials," Proc. SPIE **2114**, 444–468 (1994).
11. V. Nathan, A. H. Guenther, and S. S. Mitra, "Review of multiphoton absorption in crystalline solids," J. Opt. Soc. Am. B **2**(2), 294–316 (1985).
12. T. Kawamori, P. G. Schunemann, V. Gruzdev, *et al.*, "High-order (N = 4 - 6) multiphoton absorption and mid-infrared Kerr nonlinearity in GaP, ZnSe, GaSe, and ZGP crystals," APL Photonics **7**(8), 086101 (2022).
13. N. M. Mbhiti, G. Tóth, Z. Tibai, *et al.*, "Investigation of terahertz pulse generation in semiconductors pumped at long infrared wavelengths," J. Opt. Soc. Am. B **39**(10), 2684–2691 (2022).
14. R. S. Weis and T. K. Gaylord, "Lithium niobate: Summary of physical properties and crystal structure," Appl. Phys. A **37**(4), 191–203 (1985).
15. A. R. Zanatta, "The optical bandgap of lithium niobate (LiNbO3) and its dependence with temperature," Results Phys. **39**, 105736 (2022).
16. K. Lengyel, Á. Péter, L. Kovács, *et al.*, "Growth, defect structure, and THz application of stoichiometric lithium niobate," Appl. Phys. Rev. **2**(4), 040601 (2015).

Optics EXPRESS

17. F. Bach, M. Mero, M.-H. Chou, *et al.*, "Laser induced damage studies of $LiNbO_3$ using 1030-nm, ultrashort pulses at 10-1000 kHz," Opt. Mater. Express **7**(1), 240–252 (2017).
18. J. Hebling, A. G. Stepanov, G. Almási, *et al.*, "Tunable THz pulse generation by optical rectification of ultrashort laser pulses with tilted pulse front," Appl. Phys. B **78**(5), 593–599 (2004).
19. H. M. O'Bryan, P. K. Gallagher, and C. D. Brandle, "Congruent composition and Li-rich phase boundary of $LiNbO_3$," J. Am. Ceram. Soc. **68**(9), 493–496 (1985).
20. M. Sheik-Bahae, A. A. Said, T. Wei, *et al.*, "Sensitive measurement of optical nonlinearities using a single beam," IEEE J. Quantum Electron. **26**(4), 760–769 (1990).
21. O. Beyer, D. Maxein, K. Buse, *et al.*, "Femtosecond time-resolved absorption processes in lithium niobate crystals," Opt. Lett. **30**(11), 1366–1368 (2005).
22. H. P. Li, J. K. Liao, X. G. Tang, *et al.*, "Three-photon absorption in MgO-doped $LiNbO_3$ crystal," in *CLEO/QELS 2008* JWA35 (2008).
23. I. Steinberg, A. Kirpichnikov, and V. Atuchin, "Two-photon absorption in undoped $LiTaO_3$ crystals," Opt. Mater. **78**, 253–258 (2018).
24. M. C. Hoffmann, K.-L. Yeh, J. Hebling, *et al.*, "Efficient terahertz generation by optical rectification at 1035 nm," Opt. Express **15**(18), 11706–11713 (2007).
25. M. V. Tsarev, D. Ehberger, and P. Baum, "High-average-power, intense THz pulses from a $LiNbO_3$ slab with silicon output coupler," Appl. Phys. B **122**(2), 30 (2016).
26. M. Yin, H. Li, S. Tang, *et al.*, "Determination of nonlinear absorption and refraction by single Z-scan method," Appl. Phys. B **70**(4), 587–591 (2000).
27. B. Monoszlai, P. S. Nugraha, G. Tóth, *et al.*, "Measurement of four-photon absorption in GaP and ZnTe semiconductors," Opt. Express **28**(8), 12352–12362 (2020).
28. L. Pálfalvi, J. Hebling, G. Almási, *et al.*, "Nonlinear refraction and absorption of Mg doped stoichiometric and congruent $LiNbO_3$," J. Appl. Phys. **95**(3), 902–908 (2004).
29. A. Gaur, H. Syed, B. Yendeti, *et al.*, "Experimental evidence of two-photon absorption and its saturation in malachite green oxalate: a femtosecond Z-scan study," J. Opt. Soc. Am. B **35**(11), 2906–2914 (2018).
30. L. Pálfalvi, J. Hebling, J. Kuhl, *et al.*, "Temperature dependence of the absorption and refraction of Mg-doped congruent and stoichiometric LiNbO3 in the THz range," J. Appl. Phys. **97**(12), 123505 (2005).
31. F. Z. Henari, K. Cazzini, F. ElAkkari, *et al.*, "Beam waist changes in lithium niobate during Zscan measurement," J. Appl. Phys. **78**(2), 1373–1375 (1995).
32. F. Freytag, G. Corradi, and M. Imlau, "Atomic insight to lattice distortions caused by carrier self-trapping inoxide materials," Sci. Rep. **6**(1), 36929 (2016).
33. B. Sohn, M. Kang, J. W. Choi, *et al.*, "Observation of very high order multi-photon absorption in GeSbS chalcogenide glass," APL Photonics **4**(3), 036102 (2019).
34. D. F. Nelson and R. M. Mikulyak, "Refractive indices of congruently melting lithium niobate," J. Appl. Phys. **45**(8), 3688–3689 (1974).
35. O. Gayer, Z. Sacks, E. Galun, *et al.*, "Temperature and wavelength dependent refractive index equations for MgO-doped congruent and stoichiometric LiNbO3," Appl. Phys. B **91**(2), 343–348 (2008).
36. G. D. Boyd, R. C. Miller, K. Nassau, *et al.*, "LiNbO3: an efficient phase matchable nonlinear optical material," Appl. Phys. Lett. **5**(11), 234–236 (1964).
37. M. Nakamura, S. Higuchi, S. Takekawa, *et al.*, "Optical damage resistance and refractive indices in near-stoichiometric MgO-doped LiNbO3," Jpn. J. Appl. Phys. **41**(Part 2, No. 1A/B), L49–L51 (2002).